

Large Scale Structures in the Las Campanas Redshift Survey and in Simulations

V. Müller

*Astrophysikalisches Institut Potsdam, An der Sternwarte 16, D-14482
Potsdam, Germany*

A.G. Doroshkevich

*Theoretical Astrophysics Center, Juliane Maries Vej 30, DK-2100
Copenhagen Ø, Denmark*

J. Retzlaff

*Max-Planck-Institut f. extraterrestrische Physik, Giessenbachstrasse,
D-85740 Garching*

V. Turchaninov

*Keldysh Institute of Applied Mathematics, Russian Academy of
Sciences, 125047 Moscow, Russia*

Abstract.

The large supercluster structures obvious in recent galaxy redshift surveys are quantified using an one-dimensional cluster analysis (core sampling) and a three-dimensional cluster analysis based on the minimal spanning tree. The comparison with the LCRS reveals promising stable results. At a mean overdensity of about ten, the supercluster systems form huge wall-like structures comprising about 40% of all galaxies. The overdense clusters have a low mean transverse velocity dispersion of about 400 km/s, i.e. they look quite narrow in redshift space. We performed N-body simulations with large box sizes for six cosmological scenarios. The quantitative analysis shows that the observed structures can be understood best in low density models with $\Omega_m \leq 0.5$ with or without a cosmological constant.

1. Introduction

Very large structures in the universe as the great attractor (Dressler et al. 1988) or the great wall (Ramella, Geller, & Huchra 1992) were firstly considered as rare peculiarities in the large scale galaxy distribution. But recently published rich galaxy redshift catalogues as the Durham/UKST Galaxy Redshift Survey (Ratcliffe et al. 1996) and the Las Campanas Redshift Survey (LCRS) (Schechter et al. 1996) have established the existence of similar large structures as a typical characteristic of the galaxy distribution. They correspond to the superclusters first identified in the distribution of clusters of galaxies (Abell, 1958;

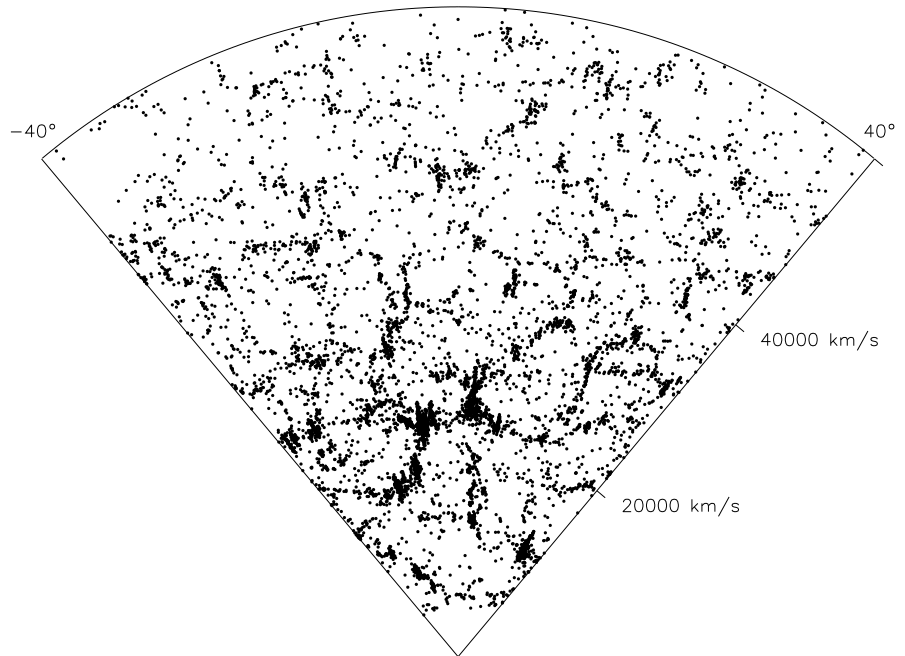


Figure 1. Wedge diagram of 80° width and 1.5° depth of a mock catalog for the magnitude limited LCRS (7500 galaxies with $15 < m < 18$.)

Oort, 1963), and we shall call them in the following simply superclusters. These structures exhibit a clear filamentary network, and the filaments seem to occupy very large wall-like regions (Doroshkevich et al. 1996). The high density superclusters incorporate $\sim 40\%$ of all galaxies, and they have a typical diameter of $\sim 30h^{-1}\text{Mpc}$ (Hubble parameter h in units of $100 \text{ km s}^{-1} \text{ Mpc}^{-1}$). They surround huge underdense regions of diameter $(50 - 70)h^{-1}\text{Mpc}$.

The appearance of such a supercluster distribution is a typical outcome of the nonlinear gravitational instability as described by the Zel'dovich theory (e.g. Shandarin & Zel'dovich, 1989). The filamentary galaxy distribution has been characterized as forming a cosmic web with a sponge like structure (Bond et al. 1996). A quantitative analysis shows that the characteristics of very large structures and the evolution history are quite sensitive to the specific cosmological model. In particular, the wall like structures are formed during a short evolution stage, and later they disintegrate into a system of high density clumps (Doroshkevich et al. 1997). The large scale matter distribution can be traced back to the initial peculiar gravitational potential (Madsen et al. 1998). Using statistical characteristics of the potential in different cosmological scenarios, the formation and evolution of the supercluster structures can be described quantitatively (Demiański & Doroshkevich 1998). These theoretical predictions and our numerical experiments can be used to constrain cosmological scenarios which give rise to the various peculiar potential fields.

We concentrate on a quantitative characterization of the geometrical properties of the supercluster structures. We take up the attempts of Babul & Starkman (1992) and Luo & Vishniac (1995) to quantify the linearity and planarity of the galaxy clustering with moments of the tensor of inertia. These statistics alone do not strongly discriminate between different cosmological models, since they characterize the general character of the anisotropic gravitational collapse. We perform a cluster analysis separately in high-density and low-density regions of the universe (the demarkation line lies about at an overdensity 10, see below), and we provide characteristics of the clusters and superclusters in dependence of the linking length used to define it. Our basic results lead to a remarkable discrimination between rich structure elements and low density regions in the universe. Recently, specific filament finders are investigated (Davé et al. 1997) which are able to follow the cosmic web. This statistic is strongly restricted to the small scale galaxy distribution. It discriminates marginally between different scenarios of structure formation, but no specific model is clearly favoured in the analysis of the CfA redshift survey. Here we employ the core sampling approach and the minimal spanning tree to define and to characterize the wall-like and the filamentary structures and to measure the parameters of their sizes, abundances and distributions.

First we provide a description of the simulations for modeling the supercluster distribution. Next we describe the cluster analysis and minimal spanning tree techniques used to analyse it. Then we employ the core sampling approach to characterize the supercluster structures in comparison to the LCRS. Finally we compare quantitative characteristics of the supercluster structures in dependence on theoretical predictions, and we discuss the results. More details can be found in Doroshkevich et al. (1998).

2. Simulating the large scale structure

We study the large scale matter distribution in N-body simulations using some of the promising cosmological scenarios presently under discussion. We use six cosmological models: A COBE normalized CDM model with density parameter $\Omega_m = 1$ (SCDM) is taken as a comparison model despite of its well known difficulties. Alternatives based on CDM and a flat geometry of the universe include modifications of the primordial power spectrum by introducing a tilt $\propto k^{0.9}$, or a break in the power spectrum at a certain scale, TCDM and BCDM, respectively. Both are inflation motivated (Gottlöber et al. 1991, 1994). Further we use open CDM models with $\Omega_m = 0.5$ and $\Omega_m = 0.35$, OCDM1 and OCDM2. Furthermore we take a model with $\Omega_0 = 0.35$ and a cosmological constant to provide spatial flatness, Λ CDM. All models are COBE normalized (Gorski et al. 1994, Stompor 1995), the amplitude is characterized by the mass variance σ_8 on a scale of $8h^{-1}$ Mpc as given in Table 1.

The simulations were run in boxes of very large comoving side length $L_{box} = 500h^{-1}$ Mpc to include with high statistics the range of wave numbers $k^{-1} \approx (10 - 30) h^{-1}$ Mpc responsible for the supercluster formation. We use a PM code, described in more detail in Kates et al. (1995). We use $N_p = 300^3$ particles in $N_{cell} = 600^3$ grid cells, which provides a force resolution $\sim 0.9h^{-1}$ Mpc, the mass resolution is given by m_p in the Table 1. For later reference, we show also

Table 1. Parameters of simulations.

model	Ω_m	h	m_p $10^{11}M_\odot$	σ_8	σ_{vel} km/s	τ_0	l_0 $h^{-1}\text{Mpc}$
SCDM	1	0.5	3.2	1.37	1375	13.2	0.6
TCDM	1	0.5	3.2	1.25	1293	13.2	0.57
BCDM	1	0.5	3.2	0.60	714	13.2	0.31
OCDM1	0.5	0.6	1.6	0.74	550	22.	0.14
OCDM2	0.35	0.65	1.1	0.57	372	29.	0.14
Λ CDM	0.35	0.7	1.1	1.12	913	26.9	0.2

the velocity dispersion of the matter particles σ_{vel} in the different simulations, which are scaled to the present time according to the linear perturbation theory. A length scale l_0 and a dimensionless constant τ_0 characterize the typical scale of the supercluster structures, and their evolution stage as discussed below:

$$l_0^{-2} = \int_{k_{min}}^{k_{max}} k^1 T(k) dk, \quad \tau_0 = \frac{\sigma_{pvel}}{\sqrt{3}l_0H_0}.$$

Here k is the comoving wave number, the factor k^1 stems from the input primordial Harrison-Zel'dovich spectrum, $T(k)$ denotes the transfer function of perturbations in the different scenarios, and $k_{min} = 2\pi/L_{box}$, and $k_{max} = k_{min}N_{cell}^{1/3}$ gives the range of the spectrum realized in the simulations.

In Retzlaff et al. (1998), we employed these simulations to discuss the power spectrum of the clustering of Abell clusters. There, model clusters were identified with maxima in the smoothed density field. Now we use the dark matter particles to characterize the geometry of the superclustering. For comparison with the observed galaxy catalogues, we must allow for differences in the distribution of galaxies and dark matter. Here we start with the simple hypothesis that on large scales, the galaxy distribution follows the gross distribution of the dark matter. As shown by the mass variance of the different models, we must allow for a bias or an anti-bias in the small scale galaxy clustering to get the observed galaxy variance $\sigma_8(\text{gal}) = 1$, and to reproduce the observed galaxy-galaxy correlation function (Tucker et al. 1997). However, we show results only for the full dark matter distribution. They are independent of any additional assumptions on prescriptions for the ‘galaxy identification’. Effectively, we employ mass cuts in the cluster definitions which are equivalent to a biasing. For producing ‘galaxy catalogues’ we also employed simple local bias prescriptions depending on the environmental density. Our conclusions are basically unchanged by such a biasing. The reason is that we study the geometrical properties of the matter distributions on very large scales which are independent on differences of the clustering of dark matter and galaxies in high density clumps.

To illustrate the simulations, we show in Fig. 1 a cone diagram of a mock ‘galaxy sample’ for the LCRS which is based on Λ CDM. We took the Schechter function of the LCRS-galaxies and assigned randomly luminosities to the dark matter mass particles according to the Schechter function characterizing the LCRS (Lin et al. 1996). Obviously, huge overdense regions are seen which match properties of the real observations.

3. Geometric characterization of large scale structures

The cluster analysis is widely used in cosmology both to define virialised objects, and for large linking lengths, to describe characteristics of the large scale matter distribution up to percolation, cf. e.g. Sahni & Coles (1995). It is closely related to the characterization of the galaxy distribution by the minimal spanning tree (MST, cf. Barrow et al. 1985). The MST represents an unique geometric construction in the galaxy distribution which is based solely on the galaxy positions. The simplest characterization of the MST is the number distribution of the edge length, $W_{MST}(l)$. First, Barrow et al. (1985) constructed it for the CfA-catalogue. At small separations, this distribution characterizes the non-linear galaxy clustering, and on large scales, it provides a measure of the topology of the geometrical support of the galaxy distribution. For random particles situated on two-dimensional (walls) or one-dimensional structures (filaments), we get logarithmic increments in the number of edge length of two and one, respectively. Parametrising the edge length distribution by

$$W_{MST}(x) = -W_0 \frac{dF_f}{dx} e^{-F_f(x)}, \quad x = l / \langle l \rangle,$$

where l denotes the edge lengths of the MST and $\langle l \rangle$ its mean. W_0 provides the normalization and the function $F_f(x)$ is parametrised as

$$F_f(x) = (\beta_1 x^{p_1} + \beta_2 x^{p_2})^{p_3}.$$

As mentioned, we are mainly interested in the effective power index $p(x) = d \log F_f / d \log x$, characterizing the geometry of the galaxy distribution.

Splitting off the MST at different linking lengths, we get standard friends-of-friends clusters with various linking lengths r_{link} , the number of clusters $N_{cl}^t(r_{link})$ (the exponent t is used to indicate on the total number of clusters, we discuss separately also clusters with different multiplicity, singlets N_{cl}^s , doublets etc.):

$$N_{cl}^t(r_{link}) = \int_{r_{link}}^{\infty} W_{MST}(l) dl.$$

Table 2. Power law indices of cluster numbers and MST edge lengths in the Λ CDM model, TOT, RSE, and LDR denote total sample, rich structure elements, and low-dense regions, respectively; com in comoving and red in redshift space.

sample	f_p	$\langle n_p \rangle$ $h^3 Mpc^{-3}$	p^s	p^t	$\langle l_{MST} \rangle$ $h^{-1} Mpc$	p^{MST}
TOT-com	1.0	0.113	0.71 ± 0.02	0.59 ± 0.03	0.72	0.60 ± 0.02
TOT-red	1.0	0.113	0.76 ± 0.02	0.85 ± 0.04	0.78	0.91 ± 0.03
RSE-red	0.45	1.86	1.82 ± 0.02	1.83 ± 0.03	0.42	1.60 ± 0.04
LDR-red	0.55	0.065	1.01 ± 0.02	1.11 ± 0.02	1.00	1.11 ± 0.03

In Table 2 we provide the power law exponents of the edge length distributions of the MST (p^{MST}) and of the cluster number versus linking length (p^s)

for singlet clusters, p^t for complete clusters) in simulated dark matter distributions of the Λ CDM model as a typical example. We show the results in the physical space and, to allow a comparison with the data from observed redshift catalogues, in redshift space, where the galaxy positions are shifted along one axis according to their peculiar velocities. In addition we use a linking length l_{link} of $1 h^{-1}\text{Mpc}$ and a threshold multiplicity $N^{thr} = 200$ for discriminating rich structure elements (RSE) with a minimum overdensity. Effectively this determines those particles in the simulations which mark ‘superclusters’ in the galaxy distribution. The remaining particles are separately analysed, they form low-density regions (LDR) which are characterized by field galaxies. The same discrimination was made by Doroshkevich et al. (1996) in the Las Campanas Redshift Survey. Similar as in the galaxy data, we identify a percentage $f \approx 0.40$ in rich structure elements in some cosmological models. In the simulations we find power law exponents p^s , p^t , and p^{MST} of about unity if analysed in physical space, i.e. the matter distribution is basically filamentary. In redshift space, the power laws for rich structure elements have exponents $p^t \approx 1.6$ and $p^{MST} \approx 1.8$, while again they are near unity in low-density regions. This difference is the main justification for the discrimination between different populations in the galaxy distribution. In redshift space the influence of the velocity dispersion erases the filamentary character of the matter distribution in RSE. Therefore we find an apparent particle distribution in huge wall-like structures.

In the LCRS a power index $p_t \approx p_{MST} \approx 1.7$ has been found for RSE, and $p_t \approx p_{MST} \approx 1$ for LDR and for the total sample. This is comparable with our results in redshift space. A complex inner structure of RSE is also visually seen in the LCRS which resamples the galaxy distribution in the great wall of the CfA catalog (Ramella, Geller & Huchra 1992).

4. Mean separation of filamentary and sheet-like components

The core-sampling method of Buryak et al. (1994) allows us to discriminate the filamentary and sheet-like structure elements and to find quantitative characteristics of these structures, namely, the surface density of filaments, σ_f , that is the mean number of filaments crossing a randomly oriented unit area (in $h^{-2}\text{Mpc}^2$), and the linear density of sheets, σ_s , that is the number of sheets crossing the unit length (in $h^{-1}\text{Mpc}$) of a random straight line. These parameters are equivalent to the mean separation between sheet-like structure elements, D_s , and filaments, D_f :

$$D_s = 1/\sigma_s, \quad D_f = \sigma_f^{-1/2},$$

i.e. these lengths represent the mean free path between sheet-like and filamentary structure elements.

For our analysis, 196 cylinders with a radius of $1.7h^{-1}\text{Mpc}$ were prepared. The mean number of points within the cylindrical cores amounts $\sim(400 - 600)$. The analysis was performed for 16 values of the cylinder radius, $1.7h^{-1}\text{Mpc} \geq r_{cyl} \geq 0.7h^{-1}\text{Mpc}$. The mean separation of sheet-like elements, D_s , and the surface density of the filamentary component σ_f , are plotted in Fig. 2 as function of the fraction of matter which is randomly selected. We provide results only for the OCDM1 and ΛCDM models which are the only reasonable models as the next

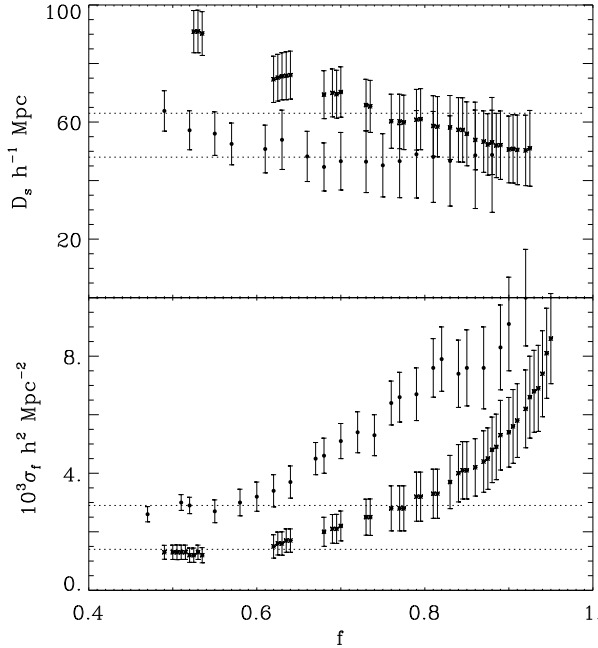


Figure 2. Mean separation of the RSE, D_s , and the surface density of filamentary component, σ_f , vs. the matter fraction concentrated within the structures, f , in redshift space for the OCDM1 (dots) and Λ CDM (stars) models.

section demonstrates. The range of values found in the LCRS (Doroshkevich et al. 1996) are marked by dotted lines. There is a clear signal from a wall-like supercluster population with a characteristic separation of $D_S \approx (40 - 60)h^{-1}$ Mpc. But in contrast with results from the observations, D_s increases slowly for small $f \leq 0.6$. This effect is probably caused by differences in the covering of the cores by the walls in the simulations, cf. also Ramella et al. (1992) and Buryak et al. (1994). On the other hand, the nearly constant $D_s(f)$ and a quick drop of σ_f with f proves that a significant matter fraction ($\sim 0.4 - 0.5$) is associated with the high dense sheet-like component, consistent with the observations.

5. Quantitative description of the overdensity regions

The discrimination of rich structure elements (RSE, or ‘superclusters’) and low-density regions (LDR populated by field galaxies) delivers no sharp criterion, we varied the linking length and the mass threshold for identifying structures. The results are shown in Fig. 3 and 4 for the various cosmological models. As discussed below, the discrimination is much more dependent on the type of cosmological model than on the exact boundary and criteria used. Therefore, the analysis delivers a test of cosmological models which is very robust.

In Fig. 3 we show the dependence of the mean overdensity of clusters on the fraction of matter in the supercluster structures. The different symbols belong to different mass thresholds (here given in terms of the minimum number of

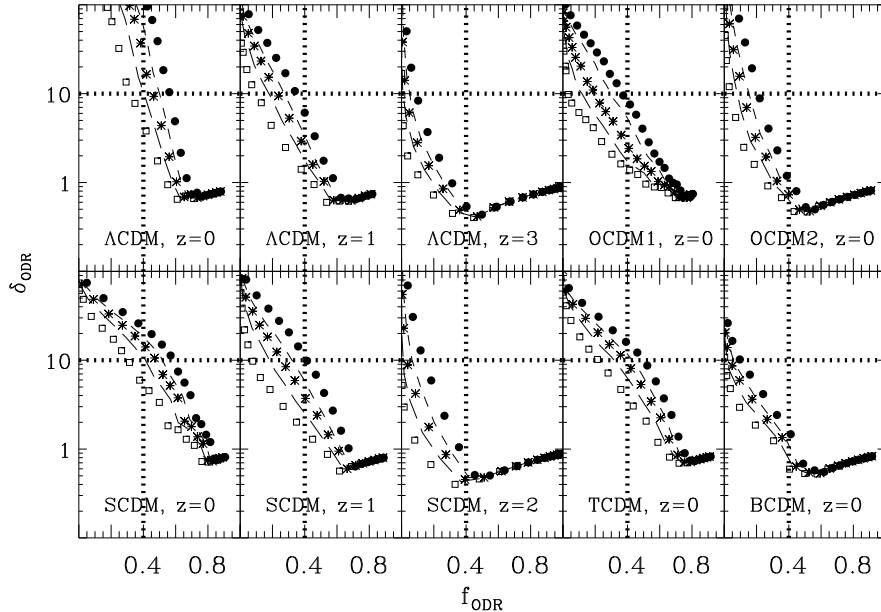


Figure 3. Overdensity δ_{ODR} in redshift space vs. matter fraction f_{ODR} for thresholds: $N_{th} = 100$ (dots), $N_{th} = 200$ (dashed line), $N_{th} = 300$ (stars), $N_{th} = 500$ (long-dashed line), $N_{th} = 1000$ (open squares). Dotted lines show the observed parameters from LCRS.

particles per cluster). The dotted lines show the approximate characteristics of the LCRS (Doroshkevich, 1996). Obviously we get rich structures in the high density regions only if the model is well evolved, in particular, OCDM2 and BCDM cannot reproduce the degree of superclustering in the LCRS.

In Fig. 4 we show the dependence of the cluster velocity dispersion along the minor axis in dependence on the fraction of matter within clusters. The velocity dispersion can be estimated from the data either using the extension of the superclusters along their smallest axis assuming virial equilibrium of the transverse galaxy motion. In this spirit, already Oort (1983) gave an estimate of the observed velocity dispersion $\sigma_v^{obs} \approx (350-400)$ km/s. The transverse velocity dispersion of superclusters in SCDM and TCDM is much too high, i.e. these models do not lead to the observed narrowness in the supercluster distribution. Also, Λ CDM shows a slight excess in the velocity dispersion along the smallest axis. The stablest superclustering is produced in OCDM1. It is remarkable that the OCDM2 models has a too low velocity dispersion and a too low concentration of matter in superclusters. This model is simply under-evolved.

For SCDM and Λ CDM we show a few evolution steps. It is obvious that the supercluster structures are built up quite recently in both models. Also the transverse velocity dispersion develops strongly due to the nonlinear gravitational clustering and the disintegration of the wall-like structures in huge filaments and high-density clumps with high and isotropic velocity dispersion. The strong evolution of the superclustering up to redshift $z = 3$ has to be compared with some observational evidence of large matter inhomogeneities at redshifts $z \approx 2 - 3$ (Connolly et al 1996, Cristiani et al 1996, Williger et al.

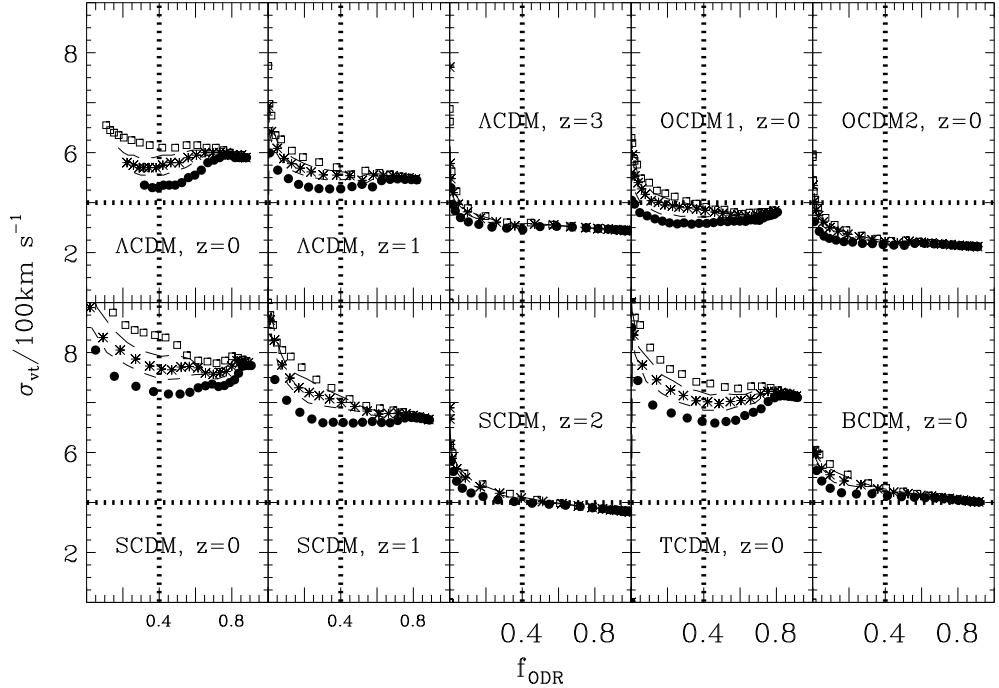


Figure 4. Velocity dispersion σ_{vt} vs. matter fraction concentrated within rich structure elements F_{RSE} for the same richness thresholds as in Fig. 3. Dotted lines show the observed parameters in the LCRS.

1996). Compared to our simulation results, such structures must be very rare at high redshifts, or there must be a strongly evolving bias of the galaxy formation up to these redshifts.

We use the eigenvalues of the tensor of inertia to estimate the degree of anisotropic gravitational collapse in forming the supercluster structures. The mean length of the rich structure elements amounts $L_1 \approx 16, 17, \text{ and } 24h^{-1}\text{Mpc}$ for SCDM, OCDM1 and ΛCDM , respectively. Along the other axes we find a collapse by a factor of two and (4–5), respectively. This is consistent with the mean overdensity of 10 for the RSE, and we expect an initial extension of the superclusters in the simulations of $L_{init}^{sim} \approx (20–25)h^{-1}\text{Mpc}$ (comoving coordinates), i.e. no collapse of the structures along the longest axis. This estimate enters in the following theoretical estimates.

6. Theoretical estimates of supercluster parameters

The reproduction of the observed characteristics of the RSE in simulations with a standard CDM-like power spectrum verifies that the observed structure may have formed during the nonlinear evolution of small initial perturbations, and that its characteristics can be derived from the parameters of the initial power spectrum of Gaussian fluctuations, and a specific cosmological model. Demiański & Doroshkevich (1998) delivered an approximate theoretical description based on Zel’dovichs nonlinear theory of gravitational instability. The comparison of

the initial size of structures, L_{init} , the wall separations, D_s , and the mean velocity dispersions in rich supercluster structures, σ_u , and the velocity dispersion along the smallest axis of the superclusters, σ_3 , are most interesting. They are connected to the length scale l_0 and evolution parameter τ_0 of the power spectrum:

$$L_{init}^{th} \approx 2.9\tau_0 l_0,$$

and for the SCDM, OCDM1 and Λ CDM models we have

$$L_{init}^{th} \approx 23h^{-1}\text{Mpc}, \quad \approx 9h^{-1}\text{Mpc}, \quad \approx 16h^{-1}\text{Mpc},$$

respectively. For the OCDM1 and Λ CDM models $L_{init}^{th} \approx (0.6 - 0.7)L_{init}^{sim}$ is found. The difference to our numerical results is caused partly by the mass threshold used, and partly by the estimates of the cluster boundary. In the SCDM model we get $L_{init}^{th} \approx 1.5L_{init}^{sim}$, it is strongly influenced by the small scale clustering.

A theoretical estimate to the mean wall separation for the mean rich superclusters is given by

$$D_s^{th} \approx 6 \cdot l_0 \sqrt{\tau_0},$$

and for the three models above we have

$$D_s^{th} \approx 56h^{-1}\text{Mpc}, \quad \approx 49h^{-1}\text{Mpc}, \quad \approx 72h^{-1}\text{Mpc},$$

respectively. These values are consistent with the values of D_s found with the core-sampling method.

The theoretical model shows that for Gaussian perturbations the distribution of the random velocity of structure elements is also Gaussian with a velocity dispersion

$$\sigma_u^{th} \approx \sqrt{3}H_0(\beta - 1)l_0\tau_0 = (\beta - 1)\sigma_{pvel}$$

where the parameter β characterizes approximately the evolutionary stage of perturbations, for SCDM $\beta = 2$, otherwise

$$\beta \approx (1 + 4\Omega_m)/(1 + 1.5\Omega_m) \approx 1.7 \quad \text{for OCDM1}$$

$$\beta \approx (1 + 3.4\Omega_m)/(1 + 1.2\Omega_m) \approx 1.54 \quad \text{for } \Lambda\text{CDM}.$$

For rich structure elements, σ_u^{th} is lower by a factor $\approx \sqrt{l_0/L_{init}^{th}} = (2.9\tau_0)^{-1/2}$. Then for SCDM, OCDM1, and Λ CDM, we have

$$\sigma_u \approx 950 \text{ km/s}, \quad 385 \text{ km/s}, \quad 490 \text{ km/s},$$

respectively. These estimates are consistent to the simulations.

A theoretical estimate for the inner velocity dispersion in RSE along the smallest axis σ_3 takes into account only the matter infall into RSE, and it ignores the disruption of the pancakes into high-density clumps. We have

$$\sigma_3^{th} \approx H_0(\beta - 1) \frac{L_{init}}{2\sqrt{3}}$$

and for a typical primordial size, L_{init}^{th} , given above,

$$\sigma_3^{th} \approx 0.5(\beta - 1)\sigma_{pvel} \approx 0.5\sigma_u.$$

This expression should be taken as a lower limit for the inner velocity dispersion, and, really, for all models under consideration, we have $\sigma_3^{th} \approx (0.5 - 0.6)\sigma_3$, i.e. the influence of small scale clustering on the properties of RSE is very important.

7. Discussion

In our analysis the properties of simulated spatial matter distributions were studied for six cosmological models with CDM-like power spectra. The simulations were performed in large boxes in order to reproduce correctly the mutual interaction of large and small scale perturbations, and to obtain a representative sample of wall-like RSE. The broad set of considered cosmological models allows us to reveal the influence of main cosmological parameters on the formation and evolution of the wall-like RSE, and to discriminate between these models. Our results show that the used methods are effective, and they yield a description of the spatial matter distribution as a whole and, in particular, the characteristics of the supercluster distribution. The main results of our analysis can be summarized as following:

- The phenomenon of the strong matter concentration of galaxies in wall-like rich structures can be reproduced with standard COBE normalized CDM-like power spectra for suitable cosmological models and simulation parameters. An essential fraction of DM, $f_{rse} \approx 0.4$, is compressed non-linearly on the scales $\sim (15 - 20) h^{-1}\text{Mpc}$ that is less than the mean separation of these RSE by a factor of $\sim 2 - 3$.
- The comparison of observed and simulated parameters of the wall-like supercluster distribution allows us to discriminate between different cosmological models. Only the low density models, the ΛCDM model with $\Omega_m h \approx 0.15 - 0.25$, or the OCDM1 model with $\Omega_m h \approx 0.25 - 0.35$ can reproduce the observed concentration of galaxies in rich superclusters. Probably, similar results can be obtained for a model with a mixture of cold and hot dark matter. A large scale bias between the spatial distribution of DM and galaxies can also improve the predictions of some models.
- Our results underline theoretical expectations concerning the epoch of the supercluster formation. At $z = 1$ the fraction of matter accumulated by superclusters with the chosen richness and overdensity drops by a factor ~ 2 , and at $z = 3$, it becomes very small.
- The simulations reproduces both the wall-like supercluster distribution and the filamentary component of the low density regions. Each component represents an essential fraction of matter in the universe, and it is equally important for the description of the joint network structure in the spatial matter distribution.

Taken together only the low density models, best OCDM1 , but also ΛCDM , can reproduce the large sheetlike matter distribution observed in recent redshift surveys.

References

- Abell G.O., 1958, *ApJ*, 3, 211
Babul A., Starkman G.D., 1992, *ApJ*, 401, 28

Barrow J., Bhavsar S., Sonoda D., 1985, MNRAS, 216, 17
 Bond J.R., Kofman L., Pogosyan D., 1996, Nature, 380, 603
 Buryak O.E., Doroshkevich A.G., Fong R., 1994, ApJ, 434, 24
 Connolly A.J., Szalay A.S., Romer A.K., et al., 1996, ApJ, 473, L67
 Cristiani S., D'Odorico S., D'Odorico V., et al. 1996, MNRAS, 285, 209
 Davé R., Hellinger D., Primack J., Nolthenius R., Klypin, A., 1997, MNRAS, 284, 607
 Demiański M., Doroshkevich, A.G., 1998, ApJ, in press
 Doroshkevich A.G., Tucker D.L., Oemler A.A., et al., 1996, MNRAS, 283, 1281
 Doroshkevich A.G., Fong R., Gottlöber S., Mückel J.P., Müller V., 1997, MNRAS, 284, 633
 Doroshkevich A.G., Müller V., Retzlaff J., Turchaninov V.I., 1998, MNRAS, submitted
 Dressler A., Faber S.M., Burstein D., et al., 1987, ApJ, 313, L37
 Gorski K.M., Hinshaw G., Bandy A.J., et al., 1994, ApJ, 431, 1
 Gottlöber S., Müller V, Starobinsky A.A., 1991, Phys. Rev. D43, 2510
 Gottlöber S., Mückel J.P., Starobinsky A.A., 1994, ApJ, 434, 417
 Kates R., Müller V., Gottlöber S., et al., 1995, MNRAS, 277, 1254
 Klypin A.A., Shandarin S.F., 1993, ApJ, 413, 48
 Lin H., Kirshner R.P., Shectman S.A., et al., 1996, ApJ, 464, 60
 Luo S., Vishniac E., 1995, ApJ Suppl., 96, 429
 Madsen S., Doroshkevich A.G., Gottlöber S., Müller V., 1998, A&A, 329, 1
 Oort J.H., 1983, Ann.Rev.Astron.Astrophys., 21, 373
 Ramella M., Geller M.J., Huchra J.P., 1992, ApJ, 384, 396
 Ratcliffe A., Shanks T., Broadbent A., et al., 1996, MNRAS, 281, L47
 Retzlaff, J., Borgani, S., Gottlöber, S., Klypin, A., Müller V., 1996, NewA, 3, 631
 Sahni, V., Coles, P., 1995, Physics Report, 262, 1
 Shectman S.A., Landy S.D., Oemler A., et al., 1996, ApJ, 470, 172
 Shandarin S., Zel'dovich Ya.B., 1989, Rev.Mod.Phys., 61, 185
 Stompor R., Gorski K.M., Bandy A.J., 1995, MNRAS, 277, 1225
 Tucker D., Oemler A., Kirshner R.P., et al., 1997, MNRAS, 285, L5
 Williger G.M., Hazard C., Baldwin J.A., McMahon R.G., 1996, ApJ Suppl., 104, 145